Imaging Local Diffusive Dynamics Using Diffusion Exchange Spectroscopy MRI

Dan Benjamini, Michal E. Komlosh, and Peter J. Basser

Phys. Rev. Lett. **118**, 158003 — Published 12 April 2017

DOI: 10.1103/PhysRevLett.118.158003

Imaging Local Diffusive Dynamics Using Diffusion Exchange Spectroscopy MRI

Dan Benjamini,[1,*] Michal E. Komlosh,[1,2] and Peter J. Basser[1]

[1] *Section on Quantitative Imaging and Tissue Sciences, NICHD, National Institutes of Health, Bethesda, MD 20892, USA*

[2] *Center for Neuroscience and Regenerative Medicine, The Henry M. Jackson Foundation for the Advancement of Military Medicine, Bethesda, MD 20892, USA*

The movement of water between microenvironments presents a central challenge in the physics of soft matter and porous media. Diffusion exchange spectroscopy (DEXSY) is a powerful 2D nuclear magnetic resonance (NMR) method for measuring such exchange, yet it is rarely used because of its long scan time requirements. Moreover, it has never been combined with magnetic resonance imaging (MRI). Using probability theory, we vastly reduce the required data, making DEXSY-MRI feasible for the first time. Experiments are performed on a composite nerve tissue phantom with restricted and free water exchanging compartments.

Water is distributed within multiple microenvironments in a variety of heterogeneous biological, geological, organic, and soft matter porous media. Nuclear magnetic resonance (NMR) and magnetic resonance imaging (MRI) are powerful tools to explore microscopic domains and pores quantitively [1–7]. In addition to providing local microscopic information, dynamic migration of water from one domain to another, referred to as molecular exchange, is important to our understanding of transport processes within these media. In petrophysics, the frequency of this exchange can reveal features of rock permeability, which is an important parameter in assessing the potential for extracting oil [8]. In biology, molecular exchange between microenvironments is directly related to cell membrane permeability and active transport processes, which are essential in understanding cellular functionality and viability [9, 10]. Measuring exchange is also valuable in soft matter applications, for example between liquid crystal domains or fluid–fluid interfaces in emulsions [5, 11].

To noninvasively measure water exchange in biological tissue using NMR and MRI, one must discriminate between MR signals arising from water in the intra- and extracellular compartments. Most NMR methods for determining membrane transport rates rely on transmembrane differences in relaxivities, namely, longitudinal and transverse relaxation rates, R_1 and R_2, respectively, or their correlation [12]. For R_1, the difference between the intra- and extracellular spaces is not sufficiently large to distinguish between them, often leading to the requirement to inject contrast agents that temporarily change the extracellular R_1 [9, 13]. For R_2, the most widely used method is relaxation exchange spectroscopy (REXSY) (first proposed by Lee et al. [14], with recent advancements [15, 16]). With REXSY, exchange can be observed based on molecular transport between pools with different R_2. However, achieving compartmental discrimination based on R_2 may also be problematic, because intra- and extracellular transverse relaxation rates are indistinguishable in many cases [17–20]. A third MR contrast mechanism, diffusion-weighted MR, noninvasively measures the microscopic net displacements of endogenous diffusing water molecules interacting with surrounding tissue, cellular, and subcellular structures [21]. These measurements provide information about the translational self-diffusion coefficient D. In complex, heterogeneous systems, several diffusion domains resulting from local water microenvironments are often present. If one assumes that intra- and extracellular are the only two compartments in biological tissue, this difference in diffusivities can be exploited for measuring exchange [22–24]. In most cases, generalization of the two-site system to model a multisite system is essential because there is often a wide distribution of exchanging compartments with different diffusion rates in biological tissue [25]. Progressing towards this goal, a recently proposed diffusion-based MRI method measured the apparent exchange rate (AXR) in a multisite system [26]. Despite these advancements, a single AXR value of multisite systems is difficult to relate to the true microscopic diffusion and exchange rates and, therefore, providing only a qualitative descriptor of exchange [26]. After laying the groundwork [3, 4], Callaghan and Furó introduced in 2004 the diffusion exchange spectroscopy (DEXSY) experiment [5]. As opposed to 1D diffusion measurements, DEXSY relies on correlating the successive diffusional motion of molecules along collinear directions, and computing a 2D map that describes these correlations. DEXSY is a model-free approach to measure exchange directly, theoretically allowing for any number of exchange processes between any number of compartments. As powerful as it is, it involves inverting a Fredholm integral of the first kind, which normally requires large amounts of acquired data due to the ill-posed nature of the problem [27, 28]. Despite its great potential, DEXSY has been used in a relatively small number of studies since its introduction [5, 27–31], conceivably due to the requirements for large amounts of data that leads to exceptionally long scan times. MRI is more time demanding than NMR because of the additional spatial encoding, precluding any DEXSY-MRI applications to date. For example, a human brain MRI would require a

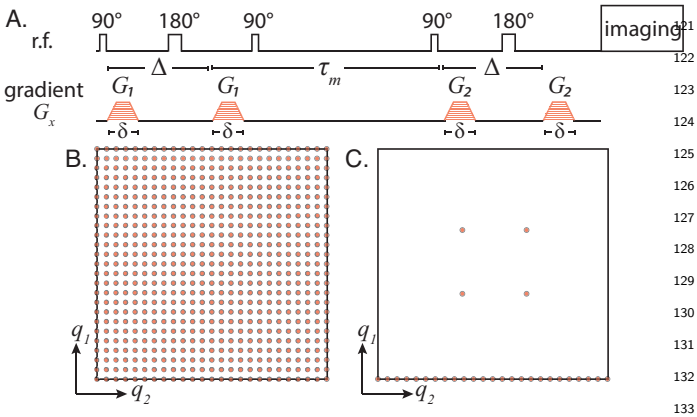

FIG. 1: Pulse sequence and acquisition schemes. (A) The pulse sequence based on two collinear PGSEs separated by a mixing time, τ_m. Schematic illustration of the data sampling strategies using (B) conventional and (C) MADCO approaches to obtain the 2D correlation function, $\mathcal{F}(D_1, D_2)$.

minimal scan time of ∼1 minute per diffusion encoding acquisition [32], while DEXSY typically requires an order of a 1000 acquisitions at a single mixing time (the time in which the exchange is allowed to occur). From a series of DEXSY maps acquired with different mixing times, the exchange rates can be deduced, leading to data collection periods of more than 15 hours per a single mixing time. In many cases biological, preclinical, and clinical MRI involve *in vivo* measurements, and are therefore limited in time – typically 10 minutes for clinical scans, 40–60 minutes for human neuroscience research, and up to 180 minutes for small animals. Here we propose a method to vastly reduce the number of required acquisitions, making DEXSY NMR and MRI possible in a wide range of applications for the first time, and taking a step toward clinical feasibility of DEXSY-MRI scanning.

Before addressing 2D diffusion exchange experiments, we consider the more common 1D diffusion experiment, pulsed gradient spin-echo (PGSE) [33]. In this technique, a pair of magnetic PGSEs of duration δ and amplitude G are used to encode the positions of precessing nuclear spins at two different times, and in opposite senses [1]. This leads to a distribution of precessional phase shifts that is characteristic of the spin displacements over the time period Δ between the pulses. It is convenient to use the definition of $q = \gamma G\delta$ as the wave vector amplitude of the gradient pulses, with γ being the gyromagnetic ratio [34]. The signal decay with q sampled over an extended range in the same direction showed a decidedly non-monoexponential behavior in heterogeneous samples [25, 35] and can therefore be expressed as

$$E(q) = \int_0^\infty \mathcal{F}(D)\,\mathcal{K}(q, D)\,\mathrm{d}D, \tag{1}$$

where each subpopulation of molecules is characterized by a local diffusivity with a probability distribution $\mathcal{F}(D)$. The function $\mathcal{K}(q, D)$, which depends on the diffusion encoding, relates q and D and is called the kernel. The effect of diffusional displacements on the PGSE experiment is to impart Gaussian distributions of phase shifts, which in turn lead to an exponential decay of the subpopulation spin echo amplitude, and in the case that $\Delta \gg \delta$, the kernel is $\mathcal{K}(q, D) = \mathrm{e}^{-q^2\Delta D}$.

In the 2D variant of the PGSE, two diffusion encoding blocks separated by a mixing time, τ_m (Fig. 1A), provide information regarding the correlation of successive displacements of the same molecule [36, 37]. It was previously used to study 2D diffusion correlations [5, 38, 39], and in conjunction with MRI to measure axon diameter [40, 41] and diameter distribution in nerve tissue [42]. In this case, Eq. 1 becomes

$$E(q_1, q_2) = \int_0^\infty \int_0^\infty \mathcal{F}(D_1, D_2)\,\mathcal{K}(q_1, q_2, D_1, D_2)\,\mathrm{d}D_1\,\mathrm{d}D_2. \tag{2}$$

When $\tau_m \gg \Delta$ the kernel is $\mathcal{K}(q_1, q_2, D_1, D_2) = \mathrm{e}^{-\left(q_1^2\Delta D_1 + q_2^2\Delta D_2\right)}$ [1]. Exchange can be measured with these 2 successive PGSE blocks by setting the directions of q_1 and q_2 to be identical and the experiment then probes changes in D over the adjustable mixing time, τ_m. D_1 is the initial diffusion coefficient obtained by the first gradients pair, while D_2 is the final diffusion coefficient of the molecules after the mixing time, measured by the second gradients pair. Conventionally, the two collinear gradient pulses pairs are stepped independently. If N 1D acquisitions are required to obtain $\mathcal{F}(D)$ from Eq. 1, an order of N^2 acquisitions will be required to resolve $\mathcal{F}(D_1, D_2)$ from Eq. 2, which is infeasible for most applications, especially *in vivo* clinical or biological MRI applications.

To achieve a considerable reduction in data acquisition requirements for the 2D experiment, we adopt concepts from probability theory, and specifically, the properties of the joint probability distribution function (PDF). Given a joint PDF, $\mathcal{F}(x_1, \ldots, x_n)$, with n variables, the PDF associated with x_i alone is defined as

$$\mathcal{F}_{X_i}(x_i) = \int \mathcal{F}(x_1, \ldots, x_n)\,\mathrm{d}x_1\,\ldots\,\mathrm{d}x_{i-1}\,\mathrm{d}x_{i+1}\,\ldots\,\mathrm{d}x_n, \tag{3}$$

and is called a marginal distribution. We may regard the diffusion exchange spectrum, $\mathcal{F}(D_1, D_2)$, as a joint probability distribution of two random variables, D_1 and D_2. Eq. 3 provides a link between the more accessible 1D information, $\mathcal{F}(D)$, and the joint PDF we are interested in finding [43]. Eqs. 1 and 2 both are examples of a broad class of Fredholm integrals of the first kind. When the kernels have an exponential form, application of an inverse Laplace transform (ILT), which is a classic ill-conditioned problem [44], is required.

The kernel and the joint PDF can be discretized on a grid with N_{D_1} and N_{D_2} values of D_1 and D_2, respectively, and N_1 and N_2 values of q_1 and q_2, respectively. One practical technique for obtaining a stable solution for $\mathcal{F}(D_1, D_2)$ is by minimizing Ξ [45, 46],

$$\Xi = \sum_{i=1}^{N_1}\sum_{j=1}^{N_2}\left[E(q_{1,i}, q_{2,j}) - \sum_{n=1}^{N_{D_1}}\sum_{m=1}^{N_{D_2}}\mathbf{F}(D_{1,n}, D_{2,m})\, \mathrm{e}^{-\left(q_{1,i}^2 \Delta D_{1,n} + q_{2,j}^2 \Delta D_{2,m}\right)}\right]^2 + \alpha \sum_{n=1}^{N_{D_1}}\sum_{m=1}^{N_{D_2}}\mathbf{F}(D_{1,n}, D_{2,m})^2, \quad (4)$$

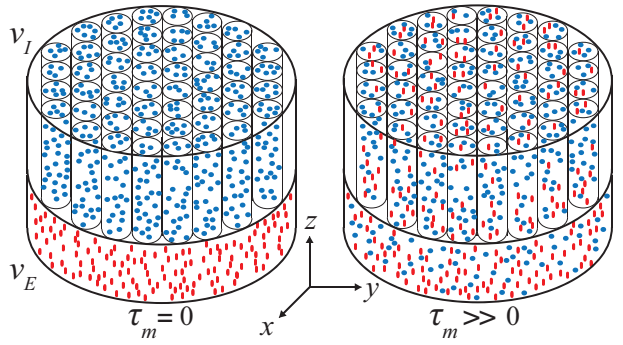

FIG. 2: Schematics of geometry and microstructure of the composite white matter phantom. As τ_m increases the fraction of water residing in v_I during the first diffusion block (blue circles) which move to v_E during the second diffusion block, and vice-versa (red lines), increases as well.

in which the first term is a data-quality term, and the second term performs Tikhonov regularization with α being the regularization parameter (the method for determining α is detailed in the Supplemental Material [47]). Here, a robust and widely used algorithm developed by Venkataramanan et al. [51, 52] was used to solve Eq. 4. Since $\mathcal{F}(D_1, D_2)$ is a PDF, nonnegativity constraints are usually imposed, such that

$$\mathbf{F}(D_1, D_2) \geq 0 \ , \forall D_{1,2}. \quad (5)$$

Resulting in vast data reduction while maintaining quality and accuracy, we recently proposed using the marginal distributions to constrain a diffusion–relaxation correlation measurement, which is a different type of a multidimensional NMR experiment [53]. These types of experiments assume that no water exchange occurs, while the current method is based on the dynamic behavior and time evolution of water transport. For exchange spectra, we note that the 1D projections of the 2D *D-D* spectrum reconstructed from DEXSY onto either the first or second dimensions are always equal to the 1D D PDF obtained from 1D diffusion measurements. Our marginal distribution constrained optimization (MADCO) framework enforces these physical constraints on the multidimensional PDF, in addition to the nonnegativity constraint. The constraints are obtained from plugging $\mathcal{F}(D_1, D_2)$ in to a discretized version of Eq. 3,

$$F(D) = \sum_{n=1}^{N_{D_1}}\mathbf{F}(D_{1,n}, D_2) = \sum_{n=1}^{N_{D_2}}\mathbf{F}(D_1, D_{2,n}). \quad (6)$$

These equality constraints are correct in an idealized system; however, expected errors in the 1D estimation of $F(D)$ require a relaxed version of Eq. 6,

$$\| \sum_{n=1}^{N_D}\mathbf{F}(D_1, D_{2,n}) - F(D)\|_2 < \sigma. \quad (7)$$

In this work we set σ to be the standard deviation of the noise (as determined after complete signal decay) normalized by the unattenuated signal and N_D. We propose that instead of sampling the entire 2D experimental parameters space (Fig. 1B) and then estimating from it the 2D distribution $\mathbf{F}(D_1, D_2)$ by minimizing Eq. 4 subject to Eq. 5, using MADCO would only require sampling along q_2, complemented with a small number of acquisitions in the 2D space (Fig. 1C). The 2D reconstruction would then have two steps: (1) estimate $F(D)$ from the 1D data, and then (2) use that estimate to constrain the estimation of $\mathbf{F}(D_1, D_2)$ by minimizing Eq. 4 subject to Eqs. 5 and 7. The exchange experiment allows us to use only a single marginal distribution as constraints, which further reduces data requirements by almost a factor of two, compared to previous publications [53, 54]).

The new DEXSY-MRI method was demonstrated by using a composite sample with two water components resembling those used to model water diffusion in white matter brain tissue [55]. The white matter phantom was comprised of a water-filled glass capillary array (GCA, Photonis, Lancaster, PA) with a nominal inner diameter of 5 μm and an open area ratio (OAR) of 0.55, along with an adjacent layer of freely diffusing water, mimicking the intra- and extracellular spaces, v_I and v_E, respectively [56] (Fig. 2). The 0.6 mm-thick imaging slice was made up of approximately 0.45 mm and 0.15 mm of GCA and free water, respectively. Water molecules in the capillaries were free to diffuse along the symmetry axis to the free water pool, and vice versa, resulting

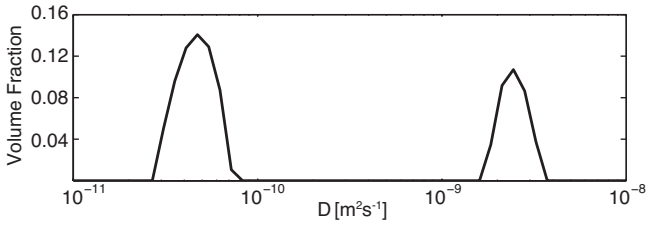

FIG. 3: The 1D diffusivity distribution, $F(D)$, obtained by solving Eq. 4 for the 1D case, using a 1D subset of the full DEXSY data. The integrated peaks represent equilibrium occupancies of f_I and f_E.

in water exchange between restricted and unrestricted compartments. The composite phantom was put in a 15 mm NMR tube and scanned on a 7 T Bruker vertical wide-bore magnet with an AVANCE III MRI spectrometer equipped with a Micro2.5 microimaging probe and three GREAT60 gradient amplifiers. DEXSY-filtered MRI data were acquired by applying the sequence in Fig. 1A followed by a 2D spin echo MRI sequence. Diffusion gradients, G_1 and G_2, were applied in the same direction (x, see Fig. 2), and their amplitudes were varied independently with $N_1 = N_2 = 45$ linear steps (resulting in $45 \times 45 = 2025$ acquisitions) in the range of 0 to 1346 mT/m, repeated with $N_{\tau_m} = 3$ mixing times, τ_m=15, 200, 300 ms, and Δ/δ of 3/15 ms/ms. MRI parameters were echo and repetition times, TE/TR, of 7.6/3000 ms/ms, a single average, in-plane nominal resolution of 0.48×0.48 mm^2, and an axial slice that included both free and restricted compartments with a thickness of 0.6 mm. All data processing was performed with in-house code written in MATLAB (The Mathworks, Natick, MA), on a D grid with $N_{D_1} = N_{D_2} = 50$.

Taking into account the OAR, the ground truth water fractions in the restricted and free compartments were $f_I^{GT} = 62\%$ and $f_E^{GT} = 38\%$, respectively. The ground truth diffusivity of the extracellular compartment was taken as water at 17° C, $D_E^{GT} = 1.8 \times 10^{-9}$ m^{2}s^{-1}. The derivation of the expected apparent diffusivity of the intra-cellular compartment, $D_I^{GT} = 4.4 \times 10^{-11}$ m^{2}s^{-1}, was based on the multiple correlation function [57] and is detailed in the Supplemental Material. Processing a 1D data subset (with G_1 set to zero) generated two distinct D contributions, shown in Fig. 3, at approximately $D_I = 4.7\times10^{-11}$ m^{2}s^{-1} and $D_E = 2.1\times10^{-9}$ m^{2}s^{-1}, for the intra- and extracellular compartments, respectively. Integration over these peaks yielded equilibrium occupancies of $f_I = 61\%$ and $f_E = 39\%$. Both diffusivities and equilibrium occupancies were in good agreement with the ground truth values.

The existence of exchange effects is clearly indicated by the presence of off-diagonal features in the DEXSY spectrum, whose position and shape give a signature for the underlying dynamics. The volume fraction of water

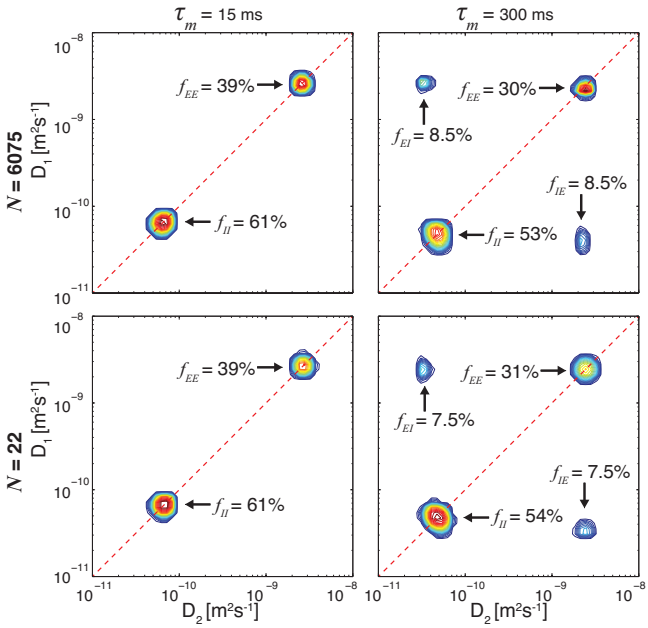

FIG. 4: DEXSY spectra. Top to bottom: obtained by using the entire data set ($N = 6075$), and by using only $N = 22$ acquisitions with MADCO. Left to right: the effect of increased τ_m, from 15 ms to 300 ms.

that remains in the v_I/v_E compartment after the mixing time is f_{II}/f_{EE} and the volume that diffused from one space to the other and vice versa is f_{IE}/f_{EI}. Processing the 2D data resulted in the $\mathbf{F}(D_1, D_2)$ spectra presented in Fig. 4. The distributions on the top row were obtained by using the entire data set, i.e., $N_1 = N_2 = 45$, $N = N_1\times N_2\times N_{\tau_m}$ (Fig. 1B). The spectra on the bottom of Fig. 4 were obtained by using only 0.35% of the data—22 acquisitions in the following manner: 1D experiment consisting of 10 steps of q_2 with $q_1 = 0$ and $\tau_m = 15$ ms, from which $F(D)$ was obtained, and additional 4 random acquisitions on the 2D grid [q_1, q_2] for each of the mixing times, i.e., $N_1 = 2N_{\tau_m}$, $N_2 = 10 + 2N_{\tau_m}$, $N = N_1 + N_2$ (Fig. 1C). It is evident from the spectra that the suggested method allowed for a vast reduction of required data, while yielding highly accurate results. As expected, f_{II}/f_{EE} decreased and f_{IE}/f_{EI} increased as a function of τ_m (Fig. 4 left to right). It is worth noting that, to this point, no *a priori* assumptions or models were used to determine the number of compartments or exchange processes. Observation of the current spectra indicates that there are two exchanging compartments and, therefore, it is possible to model the dynamic exchange process accordingly. If dictated by the DEXSY spectra, multisite exchange modeling can be applied [58]. In our case, however, the exchange is governed by the first order rate equation $\mathrm{d}f_{IE}/\mathrm{d}t = f_{II}k_{IE} - f_{IE}k_{EI}$, where k is the rate constant [11]. A similar relation governs transition from v_E to v_I simply by exchanging indices,

resulting in a set of first order equations, which along with the initial condition, $f_{IE}(\tau_m = 0) = 0$, and conservation, $f_{II} + f_{EE} + f_{IE} + f_{EI} = 1$, yields [11]

$$f_{IE}(t) = \frac{f_E k_{EI}}{k_{IE} + k_{IE}} \left[1 - \mathrm{e}^{-(k_{IE}+k_{IE})t}\right]. \qquad (8)$$

The time-dependent diagonal intensities are governed by an exponential decay with the same rate constant as for the growth of the off-diagonal peaks [31],

$$f_i(t) = f_i^0 \mathrm{e}^{-(k_{IE}+k_{IE})t} + f_i^\infty, \qquad (9)$$

with f_i representing either f_{II} or f_{EE}, and f_i^∞ is the asymptotic intensity as $\tau_m \to \infty$. Shown in Fig. 5, the integrated off-diagonal and diagonal peak intensities as a function of mixing time were fitted according to Eqs. 8 and 9 for both amounts of data, resulting in exchange rates (corrected for T_1 relaxation [11, 58]), $k = k_{IE} + k_{EI}$, of 1.76 and 1.69 s^{-1}, for $N = 6075$ and 22, respectively. When complete exchange occurred the diagonal peaks had intensities, $f_{II}^\infty / f_{EE}^\infty$, of 39%/12% and 38%/14%, and $f_{IE}^\infty = f_{EI}^\infty$ of 25% and 24%, for $N = 6075$ and 22, respectively. A comparison of the conventional and MADCO approaches showed that the DEXSY spectra, exchange rates, and complete exchange intensities were all in very good agreement. The estimated value of the intra–extracellular exchange rate was quite close to the apparent exchange rate of 1.1 s^{-1} found in *in vivo* human brain white matter [59], indicating the physiological compatibility of the currently used phantom. Since its introduction, several corrections and improvements to DEXSY have been suggested, such as addressing the case of finite mixing times, i.e., $\tau_m \sim \Delta$ [60], or correcting for possible gradient mismatch [31]. These can be readily applied by using the proposed MADCO framework.

We showed here that 22 acquisitions were sufficient to accurately determine the diffusion exchange spectrum at three mixing times. The presented framework allows one to add more mixing times at a low data requirement cost (i.e., four acquisitions per additional mixing time). Combined with a fast imaging readout, such as echo planar imaging (EPI), whole human brain imaging using 22 DEXSY acquisitions would take about 22 minutes [32], which is within the time frame of clinical MRI. Regarding the diffusion exchange spectrum as a joint probability function and accordingly imposing constraints in the optimization process, provides the opportunity to reliably and feasibly obtain spatially resolved water exchange, as reflected by physical microscopic environments. Cell membrane permeability and active transport processes in healthy and diseased tissue are only partially understood, and currently cannot be directly measured noninvasively and *in vivo*, without imposed restricting assumptions. Fast DEXSY-MRI and NMR can now be beneficial for broad application for heterogeneous materials such as biological tissues, food, plants, and rocks, providing exciting opportunities for investigators in a range of disciplines.

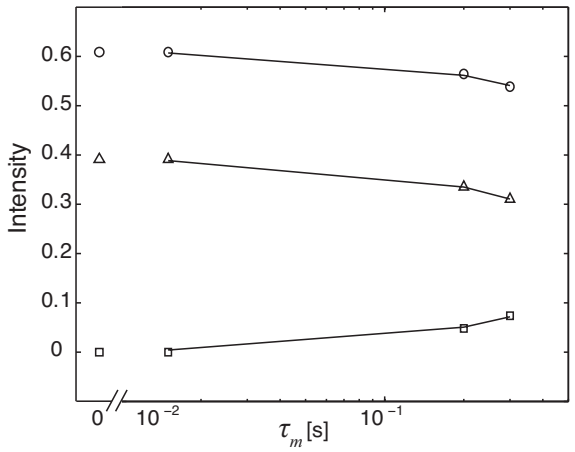

FIG. 5: Integrated intensities from the MADCO obtained spectra, f_{II} (○), f_{EE} (△), and f_{IE} (□), and their corresponding fits (–), as a function of mixing time. The 95% confidence intervals of the estimated exchange rates were $[1.47, 2.28]$ and $[1.59, 1.82]$ using the conventional and MADCO methods, respectively.

This work was supported by funds provided by the Intramural Research Program of the *Eunice Kennedy Shriver* National Institute of Child Health and Human Development (NICHD). The authors would like to thank L. Salak for editing the manuscript.

* Corresponding author: dan.benjamini@nih.gov

[1] P. Callaghan, *Principles of Nuclear Magnetic Resonance Microscopy* (Oxford University Press, New York, 1991).
[2] C. H. Arns, Physica A: Statistical Mechanics and Its Applications **339**, 159 (2004).
[3] P. T. Callaghan and M. E. Komlosh, Magnetic Resonance in Chemistry **40**, S15 (2002).
[4] P. Callaghan, S. Godefroy, and B. Ryland, Magnetic Resonance Imaging **21**, 243 (2003).
[5] P. T. Callaghan and I. Furó, The Journal of Chemical Physics **120**, 4032 (2004).
[6] W. Price, *NMR Studies of Translational Motion* (Cambridge University Press, Cambridge, 2009).
[7] P. Callaghan, *Translational dynamics and magnetic resonance: principles of pulsed gradient spin echo NMR* (Oxford University Press, 2011).
[8] L. M. Burcaw and P. T. Callaghan, Journal of Magnetic Resonance **198**, 167 (2009).
[9] J. D. Quirk, G. L. Bretthorst, T. Q. Duong, A. Z. Snyder, C. S. Springer, J. J. H. Ackerman, and J. J. Neil, Magnetic Resonance in Medicine **50**, 493 (2003).
[10] Y. Zhang, M. Poirier-Quinot, C. S. Springer, and J. A. Balschi, Biophysical Journal **101**, 2833 (2011).
[11] K. E. Washburn and P. T. Callaghan, Physical Review Letters **97**, 175502 (2006).

[12] R. D. Dortch, K. D. Harkins, M. R. Juttukonda, J. C. Gore, and M. D. Does, Magnetic Resonance in Medicine **70**, 1450 (2013).

[13] W. D. Rooney, X. Li, M. K. Sammi, D. N. Bourdette, E. A. Neuwelt, and C. S. Springer, NMR in Biomedicine **28**, 607 (2015).

[14] J. H. Lee, C. Labadie, C. S. Springer, and G. S. Harbison, Journal of the American Chemical Society **115**, 7761 (1993).

[15] M. N. D'Eurydice, E. T. Montrazi, C. A. Fortulan, and T. J. Bonagamba, The Journal of Chemical Physics **144**, 204201 (2016).

[16] R. Song, Y.-Q. Song, M. Vembusubramanian, and J. L. Paulsen, Journal of Magnetic Resonance **265**, 164 (2016).

[17] R. S. Menon and P. S. Allen, Magnetic Resonance in Medicine **20**, 214 (1991).

[18] W. A. Stewart, A. L. Mackay, K. P. Whittall, G. R. W. Moore, and D. W. Paty, Magnetic Resonance in Medicine **29**, 767 (1993).

[19] A. Mackay, K. Whittall, J. Adler, D. Li, D. Paty, and D. Graeb, Magnetic Resonance in Medicine **31**, 673 (1994).

[20] P. J. Gareau, B. K. Rutt, C. V. Bowen, S. J. Karlik, and J. R. Mitchell, Magnetic Resonance Imaging **17**, 1319 (1999).

[21] D. Le Bihan, E. Breton, D. Lallemand, P. Grenier, E. Cabanis, and M. Laval-Jeantet, Radiology **161**, 401 (1986).

[22] J. Kärger, Advances in Colloid and Interface Science **23**, 129 (1985).

[23] W. S. Price, A. V. Barzykin, K. Hayamizu, and M. Tachiya, Biophysical Journal **74**, 2259 (1998).

[24] I. Åslund, A. Nowacka, M. Nilsson, and D. Topgaard, Journal of Magnetic Resonance **200**, 291 (2009).

[25] R. V. Mulkern, H. Gudbjartsson, C. F. Westin, H. P. Zengingonul, W. Gartner, C. R. Guttmann, R. L. Robertson, W. Kyriakos, R. Schwartz, D. Holtzman, F. A. Jolesz, and S. E. Maier, NMR in Biomedicine **12**, 51 (1999).

[26] S. Lasič, M. Nilsson, J. Lätt, F. Ståhlberg, and D. Topgaard, Magnetic Resonance in Medicine **66**, 356 (2011).

[27] Y. Qiao, P. Galvosas, T. Adalsteinsson, M. Schönhoff, and P. T. Callaghan, The Journal of Chemical Physics **122**, 214912 (2005).

[28] P. Galvosas, Y. Qiao, M. Schönhoff, and P. T. Callaghan, Magnetic Resonance Imaging **25**, 497 (2007).

[29] P. L. Hubbard, K. M. McGrath, and P. T. Callaghan, Langmuir **21**, 4340 (2005).

[30] P. L. Hubbard, K. M. McGrath, and P. T. Callaghan, The Journal of Physical Chemistry B **110**, 20781 (2006).

[31] M. Gratz, M. Wehring, P. Galvosas, and F. Stallmach, Microporous and Mesoporous Materials **125**, 30 (2009).

[32] M. Lawrenz and J. Finsterbusch, Magnetic Resonance in Medicine **73**, 773 (2015).

[33] E. Stejskal and J. Tanner, Journal of Chemical Physics **42**, 288 (1965).

[34] P. T. Callaghan, C. D. Eccles, and Y. Xia, Journal of Physics E: Scientific Instruments **21**, 820 (1988).

[35] J. Pfeuffer, S. W. Provencher, and R. Gruetter, Magnetic Resonance Materials in Physics, Biology, and Medicine **8**, 98 (1999).

[36] P. Mitra, Physical Review B **51**, 15074 (1995).

[37] Y. Cheng and D. G. Cory, Journal of the American Chemical Society **121**, 7935 (1999).

[38] F. Zong, L. R. Ancelet, I. F. Hermans, and P. Galvosas, Magnetic Resonance in Chemistry (2016), 10.1002/mrc.4492.

[39] J. P. de Almeida Martins and D. Topgaard, Physical Review Letters **116**, 087601 (2016).

[40] M. A. Koch and J. Finsterbusch, NMR in Biomedicine **24**, 1422 (2011).

[41] M. E. Komlosh, E. Özarslan, M. J. Lizak, I. Horkayne-Szakaly, R. Z. Freidlin, F. Horkay, and P. J. Basser, NeuroImage **78**, 210 (2013).

[42] D. Benjamini, M. E. Komlosh, L. A. Holtzclaw, U. Nevo, and P. J. Basser, NeuroImage **135**, 333 (2016).

[43] D. Benjamini and P. J. Basser, The Journal of Chemical Physics **141**, 214202 (2014).

[44] J. G. McWhirter and E. R. Pike, Journal of Physics A: Mathematical and General **11**, 1729 (1978).

[45] R. M. Kroeker and R. Mark Henkelman, Journal of Magnetic Resonance (1969) **69**, 218 (1986).

[46] E. Fordham, A. Sezginer, and L. Hall, Journal of Magnetic Resonance, Series A **113**, 139 (1995).

[47] See Supplemental Material [url], which includes Refs. [48-50].

[48] C. H. Neuman, The Journal of Chemical Physics **60**, 4508 (1974).

[49] D. A. Yablonskiy and A. L. Sukstanskii, NMR in Biomedicine **23**, 661 (2010).

[50] H. C. Torrey, Physical Review **104**, 563 (1956).

[51] L. Venkataramanan, Y.-Q. Song, and M. Hurlimann, IEEE Transactions on Signal Processing **50**, 1017 (2002).

[52] Y.-Q. Song, L. Venkataramanan, M. Hürlimann, M. Flaum, P. Frulla, and C. Straley, Journal of Magnetic Resonance **154**, 261 (2002).

[53] D. Benjamini and P. J. Basser, Journal of Magnetic Resonance **271**, 40 (2016).

[54] D. Benjamini and P. J. Basser, Microporous and Mesoporous Materials (2017), 10.1016/j.micromeso.2017.02.001.

[55] Y. Assaf and P. J. Basser, NeuroImage **27**, 48 (2005).

[56] D. Benjamini, M. E. Komlosh, P. J. Basser, and U. Nevo, Journal of Magnetic Resonance **246**, 36 (2014).

[57] D. S. Grebenkov, Concepts in Magnetic Resonance Part A **32A**, 277 (2008).

[58] M. Van Landeghem, A. Haber, J.-B. D'espinose De Lacaillerie, and B. Blümich, Concepts in Magnetic Resonance Part A **36A**, 153 (2010).

[59] M. Nilsson, J. Lätt, D. van Westen, S. Brockstedt, S. Lasič, F. Ståhlberg, and D. Topgaard, Magnetic Resonance in Medicine **69**, 1573 (2013).

[60] J. L. Paulsen and Y.-Q. Song, Journal of Magnetic Resonance **244**, 6 (2014).